Hindawi
International Journal of Aerospace Engineering
Volume 2022, Article ID 4725423, 9 pages
https://doi.org/10.1155/2022/4725423

Research Article

Deployment Strategy and Dynamic Analysis of Large Ring Truss Antenna

Jiang Zhao, Jungang Yang, Yong Xiao, and Xiaofei Ma

Xi'an Institute of Space Radio Technology, Xi'an 710100, China

Correspondence should be addressed to Jiang Zhao; 344041630@qq.com

Received 25 April 2022; Revised 17 July 2022; Accepted 1 August 2022; Published 25 August 2022

Academic Editor: Adel Ghenaiet

The deployment strategy and dynamic analysis of the AM-2 AstroMesh ring truss antenna reflector are studied in this paper. The rigid multibody dynamic models of the truss structures with alterable and fixed diagonal length are established, respectively, by using the natural coordinate formulation (NCF). The driving scheme and the synchronous constraint scheme are proposed for two types of truss structure, respectively. The degree of freedom (DOF) analysis of the truss structure is carried out according to the redundant constraint processing method. The deployment strategies of the two different types of truss structures are discussed. The dynamic simulation of the deployment of a 30-side AM-2 AstroMesh reflector truss structure with fixed diagonal length without gravity is carried out. The deployment characteristics of the truss structure are obtained. The driving forces are predicted according to the dynamic simulation.

1. Introduction

With the rapid development of the aerospace technology, many kinds of large-scale space structures are widely used, such as deployable solar panels, deployable satellite antennas, and the large-scale deployable solar sails [1–4]. Due to the limits of space and weight of the vehicles, these large space structures must be folded up during the launch stage, and the structures deploy to the work state by the driving system after the spacecraft is in orbit. To meet the increasing space telecommunication requirements, more and more large deployable mesh antennas have been developed and applied for the aerospace missions in recent decades [5, 6].

Compared to the other structure types, the ring truss antenna has the advantage of light weight and high storage ratio. The mass of the ring truss antenna does not increase proportionally with the increase of the aperture, as shown in Figure 1. Therefore, the ring truss deployable antenna has been widely concerned by various research institutions [1, 2, 7–11].

The AstroMesh reflector, developed by the Northrop Grumman Corporation, is one of the most famous ring truss deployable antenna reflectors and has gained wide acceptance in the world of commercial satellites [8, 9]. In order to meet the requirements of the smaller fold size and the lower weight, several classes of AstroMesh reflectors such as AM-1, AM-Lite, and AM-2 have been designed and developed by Northrop Grumman Corporation based on the first generation of the AstroMesh reflector AM [12]. The AM-1 class has a reduced stowed diameter versus the first-generation AM. The AM-Lite class is also developed by optimized mass design with 50% reduction in mass from AM-1. In order to reduce the storage volume, the Northrop Grumman Corporation developed an improved mesh reflector, called AM-2, which can reduce the stowed height of the ring truss by 40% from AM-1, as shown in Figure 2 [12].

The success of deployment in orbit plays a critical role in the success of the entire space mission. Therefore, researchers have paid enough attention to the dynamic characteristics of deployment process of the ring truss antenna. Base on the second kind of Lagrange equations, Li [13] studied the deployment dynamics of a rigid ring truss structure. A five-order polynomial was used to describe the angular velocity of the deployment of the truss structure. Zhang et al. [14] studied the deployment dynamics of a simplified ring truss structure of the AstroMesh reflector by using the assumption

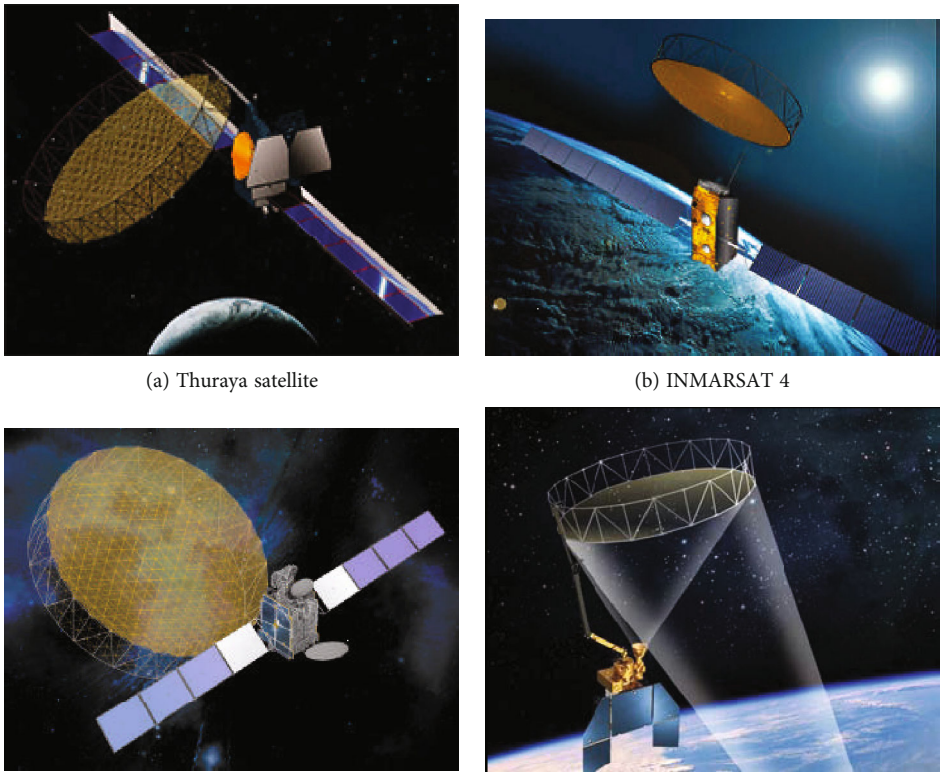

(a) Thuraya satellite

(b) INMARSAT 4

(c) MBSAT

(d) SMAP spacecraft

Figure 1: Satellite with ring truss antenna.

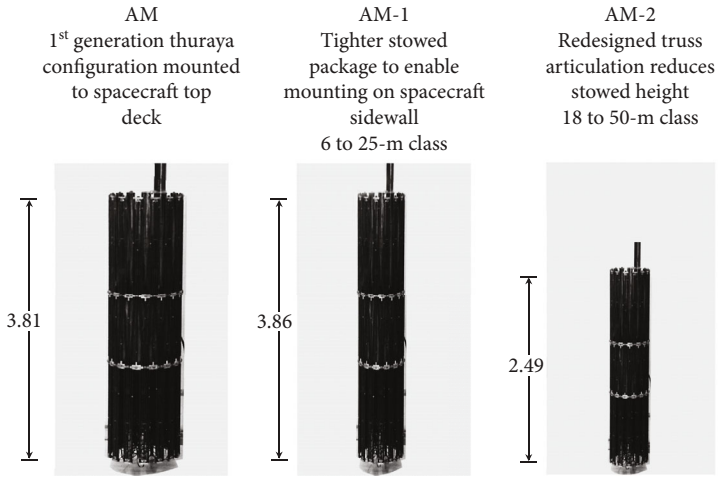

Figure 2: AstroMesh reflectors with 12-meter deployed aperture.

of small deformations and without considering the coupling effects between the rigid motion and the elastic deformation. Li et al. [15] proposed an effective form-finding methodology that combines the iterative force density method and the minimum norm method. The form-finding analysis of the reflector with the standard configuration, the central hub configuration, and the circular configuration is performed to validate the proposed methodology. Based on the initial configuration, the deployment dynamics of a complex AstroMesh reflector was studied by using the parallel computation [16]. Peng et al. [17] proposed a new cable element of ALE formulation to simulate the cable pulley system with friction and carried out the deployment simulation of a full-scale flexible multibody model of the AstroMesh. The variations of the kinetics of the structure, the bending moments of the truss members, and the motor driving forces in the deployment process are discussed.

However, most scholars focused on the AM class of AstroMesh reflectors in the dynamic characteristics research of the ring truss deployable reflector; the dynamic analysis of the AM-2 class has seldom been investigated. In this paper, the natural coordinate formulation (NCF) [16] is applied to model

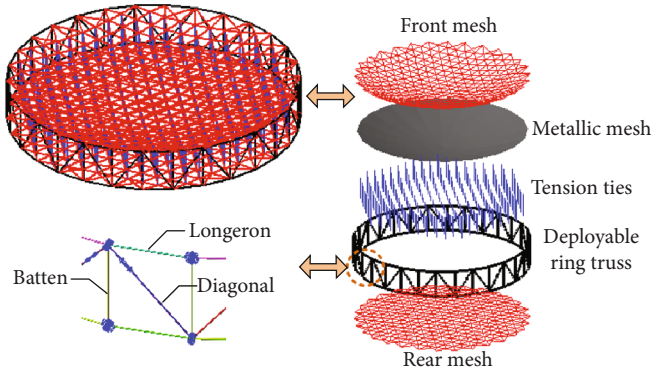

Figure 3: Components of AstroMesh reflector truss.

the ring truss deployable antenna structure. Combining the analysis of degrees of freedom (DOFs) and the dynamic simulation, the deployment strategy and dynamic analysis of the AM-2 class of AstroMesh reflectors are analyzed.

2. AstroMesh Truss Structure

The AstroMesh reflector is mainly composed of a deployable ring truss, the front net, the rear net, and tension ties. The metal mesh is attached to the front net for the reflective surface. When the deployment of the reflector is completed, the front net, the near net, and ties are all in tension. The AstroMesh reflector truss is comprised of longeron, diagonal, and batten rods, as shown in Figure 3 [15].

The AM-class of the AstroMesh truss is composed of several parallelogram elements. The diagonal in the parallelogram element is extensible mechanism. The length of the diagonal is maximum when the structure is in the folded state, and that is minimum when the structure is in the deployment state. The ring truss structure is deployed by driving the cable embedded in the diagonals of each parallelogram of the structure, as shown in Figure 4.

The AM-2 of the AstroMesh ring truss reflector is also composed of several parallelogram elements as AM. However, unlike AM, the hinge connecting the batten rod and the other rods is not fixed that can slide freely on the batten rod. The hinge slides from the bottom of the batten rod to the top during the deploying process of ring truss structure, and the hinge slides from the top of the batten rod to the bottom during the stowing process of the ring truss structure, as shown in Figure 5.

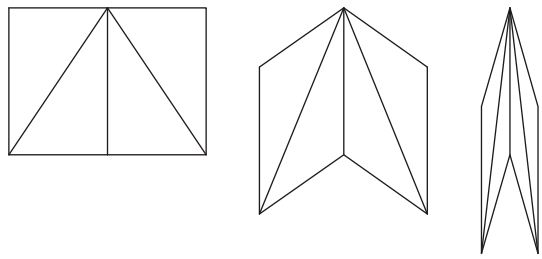

Figure 4: Parallelogram element of AM ring truss structure.

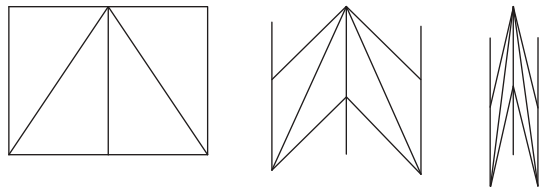

Figure 5: Parallelogram element of AM-2 ring truss structure.

3. Modeling of Truss Structure

3.1. Natural Coordinate Formulation. In the natural coordinate formulation (NCF), the Cartesian coordinates in the global inertial coordinate system are applied to define the motion of the rigid body [18]. The mass matrices in the dynamic formulations are constant. Therefore, it can greatly improve the computational efficiency in the dynamic simulation by using NCF. In this paper, two fixed points and two non-coplanar unit vectors are used as the generalized coordinates, as shown in Figure 6.

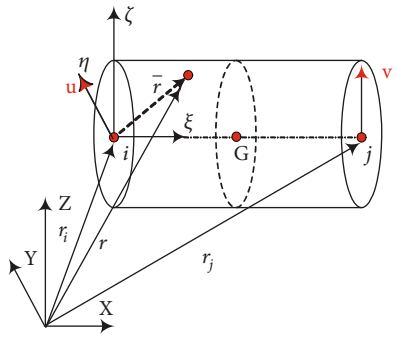

Figure 6: Rigid body described by NCF.

The rigid body has 12 generalized coordinates in the global coordinate system

$$\mathbf{q} = \left[\mathbf{r}_i^T \; \mathbf{r}_j^T \; \mathbf{u}^T \; \mathbf{v}^T\right]^T, \tag{1}$$

where $\mathbf{r}_i$ and $\mathbf{r}_j$ are the position vectors of the node i and j, respectively. The vectors $\mathbf{u}$ and $\mathbf{v}$ are two non-coplanar unit

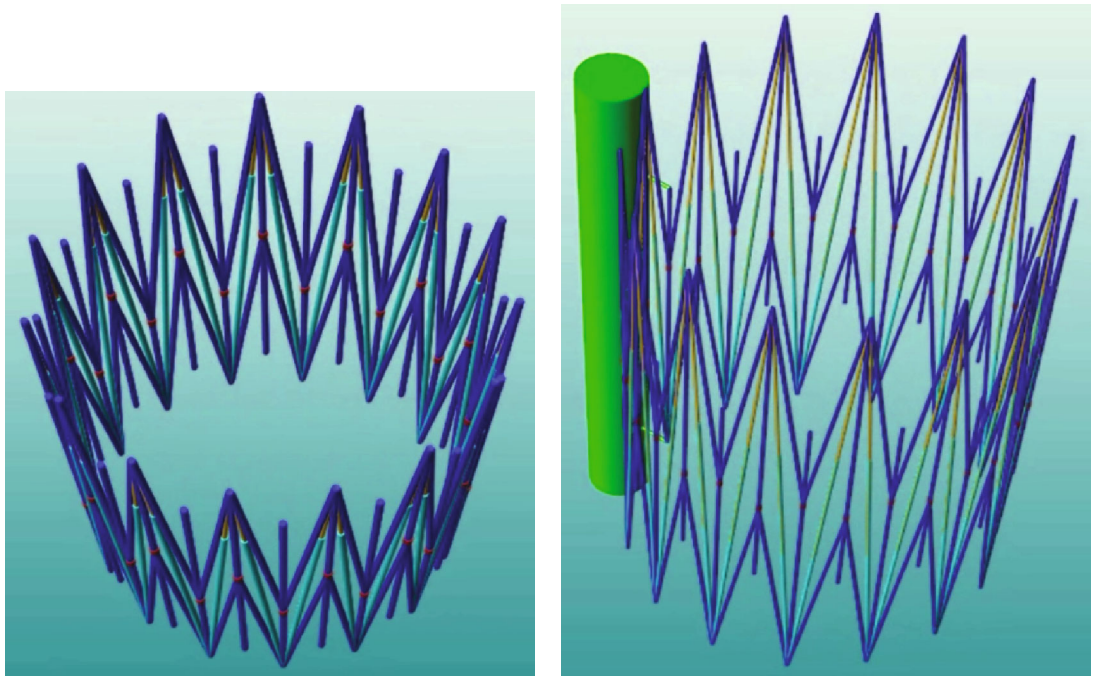

(a) Space free case (b) One batten fixed case

Figure 7: Two different cases of the ring truss structure.

Table 1: DOFs of truss structure in two cases.

Case of structure	Space free	One batten fixed
Degrees of freedom	61	55

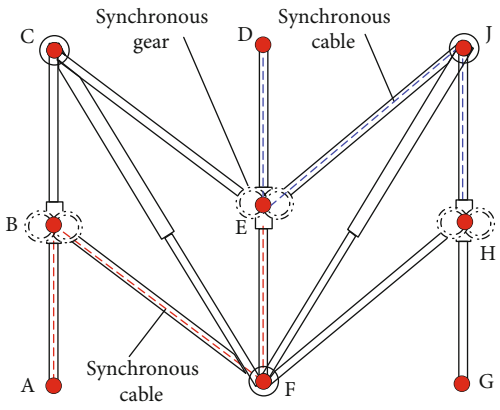

Figure 8: Truss element with synchronous constraints.

vectors. The vectors $\mathbf{r}_j - \mathbf{r}_i$, $\mathbf{u}$, and $\mathbf{v}$ are perpendicular to each other. The global position of an arbitrary point P in the rigid body can be described as

$$\mathbf{r} = [(1 - c_1)\mathbf{I}_3 \; c_1\mathbf{I}_3 \; c_2\mathbf{I}_3 \; c_3\mathbf{I}_3] \begin{Bmatrix} \mathbf{r}_i \\ \mathbf{r}_j \\ \mathbf{u} \\ \mathbf{v} \end{Bmatrix} = \mathbf{Cq}, \tag{2}$$

Table 2: DOFs of truss structure in different cases.

Case of structure	Synchronous cables	Synchronous gears	Synchronous cables and synchronous gears
Space free	34	33	8
One batten fixed	28	27	2

Table 3: DOFs of truss structure with fixed length of diagonal.

Case of structure	Without synchronous constraint	Synchronous cables
Space free	32	7
One batten fixed	26	1

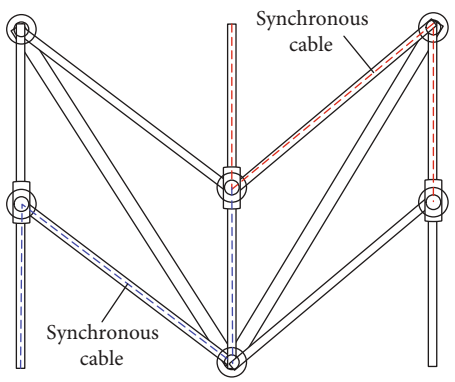

Figure 9: Truss element with synchronous cables constraints.

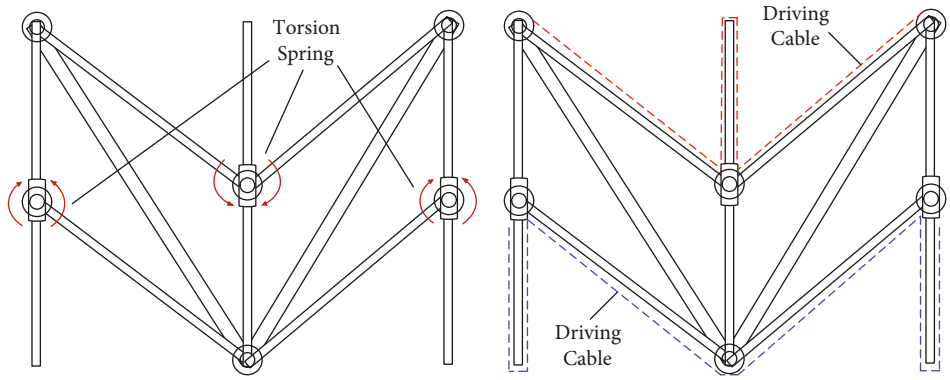

(a) Torsion spring (b) Driving cable

Figure 10: Driving scheme for the deployment of the ring truss structure.

where $\mathbf{C}$ is the shape function matrix which depends on the local coordinate of point P. $\mathbf{I}_3$ is the 3×3 identity matrix.

It is known that the rigid body has 6 degrees of freedom (DOFs) in the space. The rigid body described by NCF has 12 generalized coordinates. There are 6 inherent constraints for one rigid body, and the constraint functions can be written as

$$\begin{cases} |\mathbf{r}_i - \mathbf{r}_j| = L, \quad |\mathbf{u}| = 1, \quad |\mathbf{v}| = 1, \\ (\mathbf{r}_i - \mathbf{r}_j) \perp \mathbf{u}, \quad (\mathbf{r}_i - \mathbf{r}_j) \perp \mathbf{v}, \quad \mathbf{u} \perp \mathbf{v}. \end{cases} \tag{3}$$

3.2. Dynamic Equation of the Truss Structure. Based on the first Lagrange equation, considering the constraints, the governing equation of motion for a multibody system can be expressed in a compact form as a set of differential and algebraic equations (DAEs) with constant mass matrix

$$\begin{cases} \mathbf{M}\ddot{\mathbf{q}} + \boldsymbol{\Phi}_{\mathbf{q}}^{\mathrm{T}} \boldsymbol{\lambda} = \mathbf{Q}(\mathbf{q}, t), \\ \boldsymbol{\Phi}(\mathbf{q}, t) = \mathbf{0}, \end{cases} \tag{4}$$

where $\mathbf{M}$ represents a system constant mass matrix of the system, $\mathbf{q}$ represents the generalized coordinates of the whole multibody system, and $\boldsymbol{\Phi}(\mathbf{q}, t)$ represents the constraint vector of the system. The Jacobian matrix $\boldsymbol{\Phi}_{\mathbf{q}}$ is the derivative matrix of the constraint vector with respect to the generalized coordinates $\mathbf{q}$, $\boldsymbol{\lambda}$ is the Lagrange multiplier vector, and $\mathbf{Q}(\mathbf{q}, t)$ is the generalized external forces vector of the system.

It should be pointed out that redundant constraints are usually generated inevitably when describing the constraint equations for the complex multibody system, especially the closed-loop deployable structure. Therefore, the redundant constraints should be removed by eliminating the dependent constraint equations in the degree of freedom analysis and the dynamic analysis of the system.

The total constraint equations of a multibody system are usually composed of the inherent constraint equations such as Equation (3) and the constraint equations for the connections between the components of the structure. The Gaussian elimination method is adopted to eliminate the principal elements in the Jacobian matrix $\boldsymbol{\Phi}_{\mathbf{q}}$, and then, the independent constraint equations would be obtained after removing the corresponding redundant constraint equations. The degrees of freedom of the system can be obtained by subtracting the number of the independent constraint equations from the number of generalized coordinates.

4. DOF Analysis and Constraint Scheme

Based on this configuration with sliding hinges on the batten rods, the deployment strategy of the ring truss structure with alterable diagonal length and with fixed diagonal length is discussed, respectively, in this section.

4.1. Truss with Alterable Diagonal Length. The AM-2 type of ring truss structure with variable length of the diagonal is considered in this section. The rigid dynamic model of the ring truss structure with 30 sides in two different cases are established by using NCF introduced in Section 3.1, respectively. The rigid parts in the dynamic model include 60 longeron rods, 30 batten rods, 60 diagonal rods, and 30 sliding hinges on the batten rods. The constraint equations include the rotation joints between the longeron and the batten rods, the rotation joints between the diagonal and the batten rods, the sliding joints between the hinges and the batten rods, and the sliding joints between the diagonal rods in the same parallelogram elements.

The first case is that the truss structure is completely free in the space without any external constraint, and the second case is that one batten rod of the truss structure is fixed in the space, as shown in Figure 7. The degree of freedom of the ring truss structure is analyzed by the rigid dynamic model.

The DOFs of the truss structure are shown in Table 1. As shown in this table, the DOFs of the structure in space free case are 6 more than the DOFs of the structure in one batten fixed case as expected. It is obvious that the structure is not reliable with such numbers of DOFs as shown in the table.

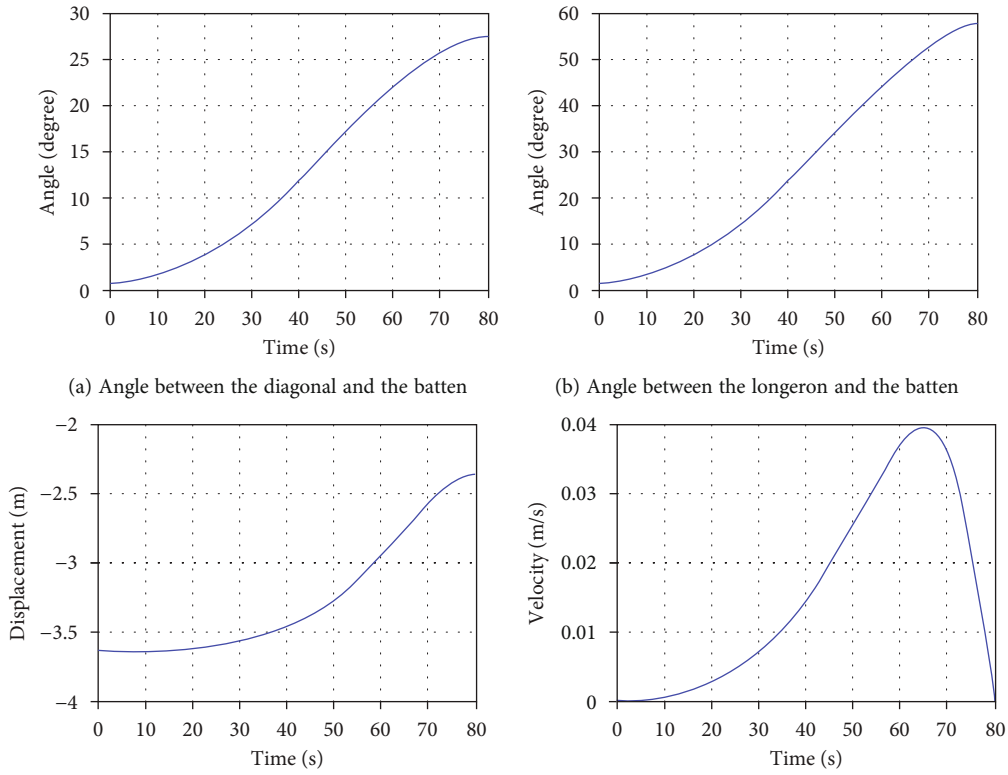

(a) Angle between the diagonal and the batten

(b) Angle between the longeron and the batten

(c) Displacement of sliding joint from the tip of the batten

(d) Velocity of sliding joint from the batten

Figure 11: Simulation results of the truss deployment in the first stage.

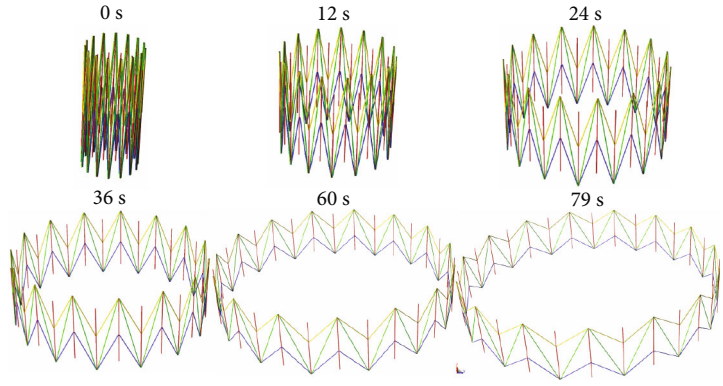

Figure 12: Deployment configurations in the first stage.

In order to reduce the DOFs of the structure and improve the deployment reliability of the truss structure, the synchronous constraints are needed for the structure which can be achieved by using the synchronous cables and the synchronous gears, as shown in Figure 8.

The synchronous cable has a constant length which is the sum of the length of the batten and the longeron rod. It can be used to control the sliding motions of two hinges in the same truss unit, and the truss units remain parallelograms in the deployment progress due to the synchronous cables. The constraint equations for the synchronous cables in Figure 8 can be described as follows:

$$\begin{cases} |\mathbf{r}_A - \mathbf{r}_B| - |\mathbf{r}_D - \mathbf{r}_E| = 0, \\ |\mathbf{r}_D - \mathbf{r}_E| - |\mathbf{r}_G - \mathbf{r}_H| = 0, \end{cases} \tag{5}$$

where $\mathbf{r}_A$, $\mathbf{r}_B$, $\mathbf{r}_D$, $\mathbf{r}_E$, $\mathbf{r}_G$, and $\mathbf{r}_H$ represent the position vectors of points A, B, D, E, G, and H in the global coordinate, respectively.

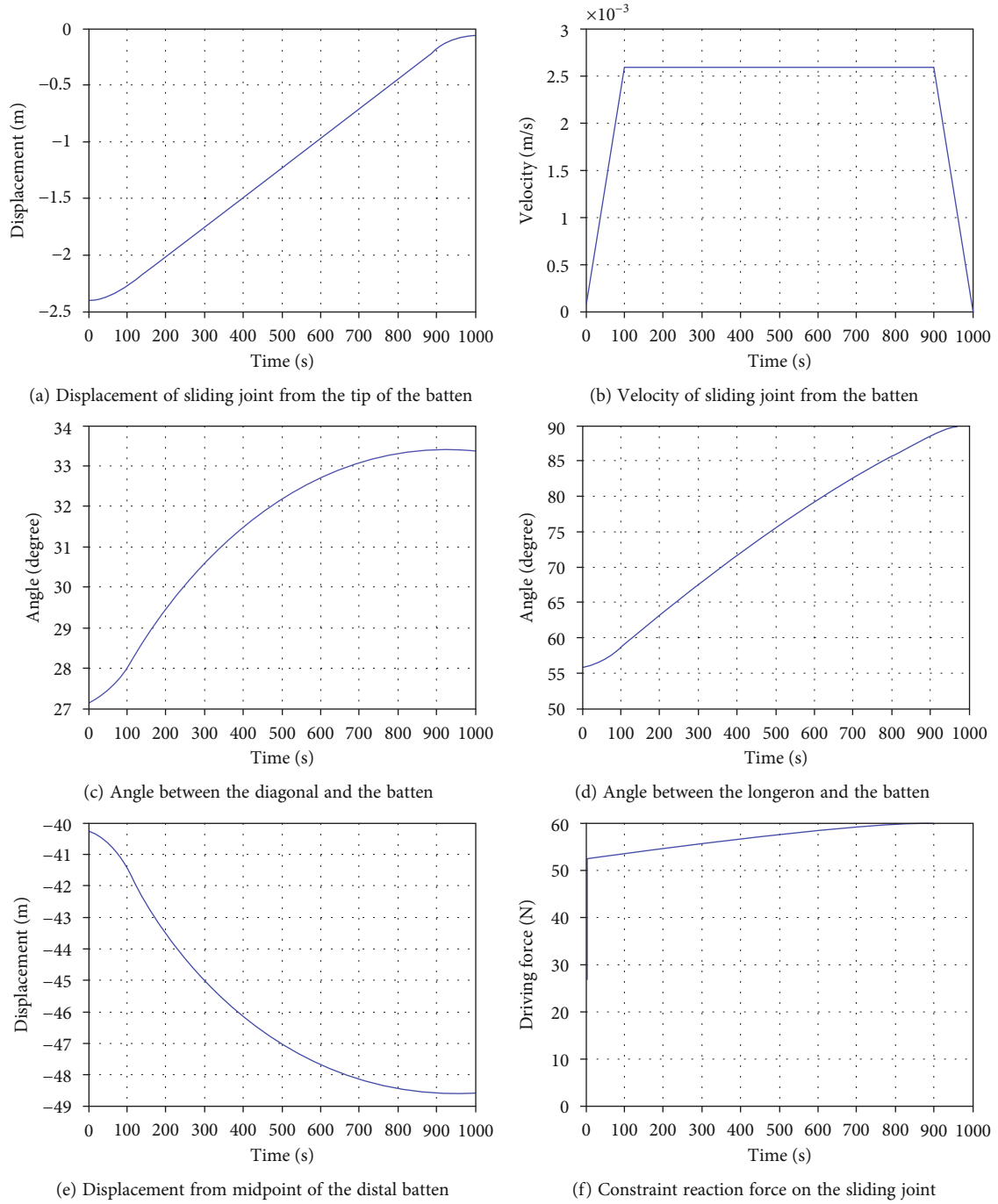

(a) Displacement of sliding joint from the tip of the batten

(b) Velocity of sliding joint from the batten

(c) Angle between the diagonal and the batten

(d) Angle between the longeron and the batten

(e) Displacement from midpoint of the distal batten

(f) Constraint reaction force on the sliding joint

Figure 13: Simulation results of the truss deployment in the second stage.

The synchronous gear is installed in the sliding hinge connecting one batten and two longeron rods, as shown in Figure 8. It can be used to control the motion of the adjacent truss units. The rotation angles of two adjacent longeron rods connecting the sliding hinge with respect to the batten rod keep consistent due to the synchronous gears. The constraint equations for the synchronous gears in Figure 8 can be described as follows:

$$\frac{(\mathbf{r}_D - \mathbf{r}_E)\cdot(\mathbf{r}_C - \mathbf{r}_E)}{|\mathbf{r}_D - \mathbf{r}_E||\mathbf{r}_C - \mathbf{r}_E|} - \frac{(\mathbf{r}_D - \mathbf{r}_E)\cdot(\mathbf{r}_J - \mathbf{r}_E)}{|\mathbf{r}_D - \mathbf{r}_E||\mathbf{r}_J - \mathbf{r}_E|} = 0, \quad (6)$$

where $\mathbf{r}_C$ and $\mathbf{r}_J$ represent the position vectors of points C and J in the global coordinate, respectively.

The rigid dynamic model of the 30-side ring truss structure with synchronous cables and synchronous gears is established by using NCF. DOF analysis of the truss structure in different cases is performed, as shown in Table 2.

It is shown from the table that the DOFs of the ring truss structure can be reduced significantly by using the synchronous constraints. If the synchronous cables and synchronous gears are applied simultaneously, the DOFs of the structure

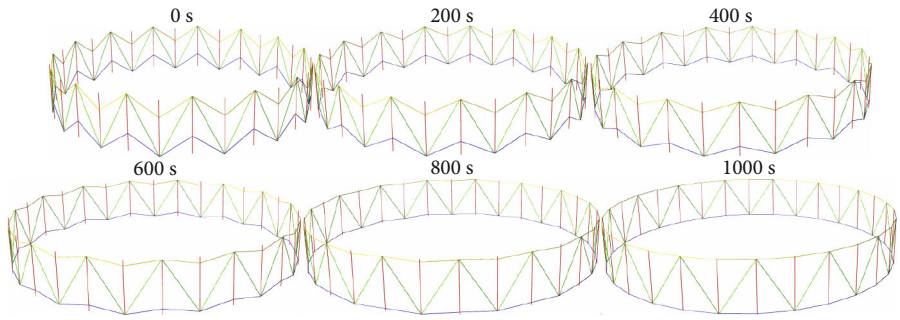

Figure 14: Deployment configurations in the second stage.

are reduced to 2 which means that the deployment reliability of the truss structure is significantly improved.

4.2. Truss with Fixed Diagonal Length. The AM-2 type of ring truss structure with fixed length of the diagonal is considered in this section. The rigid dynamic model of the ring truss structure with 30 sides in the case of space free and in the case of one batten fixed is established by using NCF, respectively. Compared with the rigid dynamic model of the truss with alterable diagonal length, this kind of rigid dynamic model has 30 fewer diagonal rods, and the constraint equations do not contain the sliding joints between the diagonal rods in the same parallelogram elements.

The degrees of freedom of the ring truss structure are analyzed by using the rigid dynamic model.

It can be seen that the DOFs of the structure with the fixed diagonal length are much less than the structure with the alterable diagonal length by comparing Tables 2 and 3. Since the length of the diagonal rods keep constant, it eliminates some of the DOFs from the truss structure. The DOFs of the truss structure with the fixed diagonal length reduce to 1 when the synchronous cables constraints are applied, as shown in Figure 9. It is obvious that this type of AM-2 truss structure has higher stability and reliability.

5. Dynamic Simulation of AM-2 Truss Structure

The dynamic simulation of the deployment of a 30-side AM-2 AstroMesh reflector truss with the fixed diagonal length without gravity is carried out in this section by using the rigid dynamic model established before. As with the AM class of AstroMesh reflectors, the deployment of the AM-2 AstroMesh reflector truss can be divided into two stages. In the first stage, the truss deploys to a semi-unfolding configuration under the action of the moments between the longeron rod and the batten rod which can be achieved by torsion springs. In the second stage, the truss deploys to the final unfolding configuration under the action of the driving forces between the hinge and the batten rod which can be achieved by the driving cables, as shown in Figure 10.

The aperture of the truss structure is 50 m. The length of the longeron and the batten rods are 5.1 m and 7.8 m, respectively. The outer diameter of the rods is 30 mm, and the thickness is 1.2 mm. The density of the material is 1600 kg/m^3. The initial rotational torque of the torsion spring is set as 3.0 Nm, and it would reduce to zero when the rotation angle reaches to 33 degrees.

As shown in Figure 11, in the first deployment stage, the deployment speed of the truss decreases to zero when the angle between the longeron and the batten rods is 56.8 degrees and the angle between the diagonal and the batten rods is 27.3 degrees. The deployment time is 79.8 s. The deployment configurations of the truss structure at different times in the first stage are shown in Figure 12.

In the second stage, in order to ensure the stability of the deployment process, the dynamic simulation of the deployment is carried out according to the constraint planning method [19]. The total time for the deployment process is set as 1000 s. The displacement and the velocity of the sliding joint on the batten rod are planned as shown in Figures 13(a) and 13(b). As shown in Figures 13(c)–13(e), the truss is gradually deployed to the final state configuration under the action of driving force. It can also be seen from the constraint reaction curves in Figure 13(f) that the maximum driving force required for truss deployment is about 60 N. The deployment configurations of the truss structure at different times in the second stage are shown in Figure 14.

6. Conclusion

According to the concept of AM-2 AstroMesh reflector truss structure, the rigid multibody system of two different types of AM-2 ring truss structure is established in this work. The system is described by using the natural coordinate formulation (NCF). The synchronous constraint schemes are proposed for the two types of truss structure, respectively. The deployment strategy of the truss structures is studied by using the degree of freedom (DOF) analysis. The results show that the DOFs of the truss structure can be reduced effectively by applying the synchronous constraints. It also can be shown from the results that the truss structure with fixed diagonal length has higher stability and reliability than the truss structure with alterable diagonal length. The dynamic simulation of the deployment of a 30-side AM-2 AstroMesh reflector truss structure with fixed diagonal length without gravity is carried out. The truss is deployed by the torsion springs and the driving cables in the first and second deployment stage, respectively. The driving forces are predicted according to the dynamic simulation. The dynamic characteristics of the deployment of the truss structure are obtained. Based on this work, the flexible

multibody dynamic model of the reflector truss would be developed for the truss structure. The mesh and tension ties can also be considered in the deployment simulation in the future work. The dynamic characteristics of the deployment of the reflector would be simulated more accurately.

Data Availability

The raw/processed data required to reproduce these findings cannot be shared at this time as the data also forms part of an ongoing study.

Conflicts of Interest

The authors declare that they have no conflicts of interest.

Acknowledgments

This work was supported in part by the National Natural Science Foundation of China under Grant Nos. 11402196 and 11290154.

References

[1] W. Thomson, "The AstroMesh deployable reflector," *IEEE Antennas and Propagation Society*, vol. 3, pp. 1516–1519, 1999.

[2] A. Meguro, S. Harada, and M. Watanabe, "Key technologies for high-accuracy large mesh antenna reflectors," *Acta Astronautica*, vol. 53, no. 11, pp. 899–908, 2003.

[3] M. A. Neto, J. A. C. Ambrosio, and R. P. Leal, "Composite materials in flexible multibody systems," *ComputerMethods in Applied Mechanics and Engineering*, vol. 195, pp. 6860–6873, 2006.

[4] Y. Miyazaki, Y. Shirasawa, O. Mori, and H. Sawada, "Finite element analysis of deployment of gossamer space structure," in *Multibody Dynamics ECCOMAS Thematic Conference*, p. 2011, Brussels, Belgium, 2011.

[5] J. M. Hedgepeth, "Accuracy potentials for large space antenna reflectors with passive structure," *Journal of Spacecraft and Rockets*, vol. 19, no. 3, pp. 211–217, 1982.

[6] S. J. Wang and J. M. Cameron, "Dynamics and control of a large space antenna," *Journal of Guidance, Control, and Dynamics*, vol. 7, no. 1, pp. 69–76, 1984.

[7] Z. You and S. Pellegrino, "Cable-stiffened pantographic deployable structures part 2: mesh reflector," *AIAA Journal*, vol. 35, no. 8, pp. 1348–1355, 1997.

[8] M. W. Thomson, "Astromesh deployable reflectors for Ku- and Ka-band commercial satellites," in *20th AIAA International Communication Satellite Systems Conference and Exhibit*, Montreal, Quebec, Canada, 2002.

[9] M. Mobrem, S. Kuehn, C. Spier, and E. Slimko, "Design and performance of AstroMesh reflector onboard soil moisture active passive spacecraft," in *Proceedings of the Aerospace Conference*, pp. 1–10, Piscataway, NJ, 2012.

[10] X. Qi, H. Huang, B. Li, and Z. Deng, "A large ring deployable mechanism for space satellite antenna," *Aerospace Science and Technology*, vol. 58, pp. 498–510, 2016.

[11] B. Li, X. Qi, H. Huang, and W. Xu, "Modeling and analysis of deployment dynamics for a novel ring mechanism," *Acta Astronautica*, vol. 120, pp. 59–74, 2016.

[12] Northrop Grumman, *AstroMesh™ Reflector Parametrics*, Northrop Grumman Corporation, 2016.

[13] T. Li, "Deployment analysis and control of deployable space antenna," *Aerospace Science and Technology*, vol. 18, no. 1, pp. 42–47, 2012.

[14] Y. Zhang, B. Duan, and T. Li, "A controlled deployment method for flexible deployable space antennas," *Acta Astronautica*, vol. 81, no. 1, pp. 19–29, 2012.

[15] P. Li, C. Liu, Q. Tian, H. Hu, and Y. Song, "Dynamics of a deployable mesh reflector of satellite antenna: form-finding and modal analysis," *Journal of Computational and Nonlinear Dynamics*, vol. 11, no. 4, article 041017, 2016.

[16] P. Li, C. Liu, Q. Tian, H. Hu, and Y. Song, "Dynamics of a deployable mesh reflector of satellite antenna: parallel computation and deployment simulation," *Journal of Computational and Nonlinear Dynamics*, vol. 11, no. 6, p. 61005, 2016.

[17] Y. Peng, Z. Zhao, J. He, J. Yang, and Y. Xiao, "Flexible multibody model and the dynamics of the deployment of mesh antennas," *Journal of Guidance, Control, and Dynamics*, vol. 40, no. 6, pp. 1499–1510, 2017.

[18] J. Garcia De Jalon and E. Bayo, *Kinematic and Dynamic Simulation of Multibody Systems the Real-Time Challenge*, Springer, New York, 1994.

[19] C. Liu, Q. Tian, and H. Hu, "Dynamics and control of a spatial rigid-flexible multibody system with multiple cylindrical clearance joints," *Mechanism and Machine Theory*, vol. 52, pp. 106–129, 2012.